European Journal of Pharmaceutics and Biopharmaceutics 165 (2021) 279–292

Contents lists available at ScienceDirect

European Journal of Pharmaceutics and Biopharmaceutics

journal homepage: www.elsevier.com/locate/ejpb

Synthesis and validation of DOPY: A new gemini dioleylbispyridinium based amphiphile for nucleic acid transfection

Eva Aubets [a,d], Rosa Griera [b], Alex J. Felix [a,d], Gemma Rigol [a], Chiara Sikorski [a,1], David Limón [b,d], Chiara Mastrorosa [a,2], Maria Antònia Busquets [c,d], Lluïsa Pérez-García [b,d,*], Véronique Noé [a,d], Carlos J. Ciudad [a,d,*]

[a] Department of Biochemistry and Physiology, School of Pharmacy and Food Sciences, University of Barcelona, 08028 Barcelona, Spain
[b] Department of Pharmacology, Toxicology and Therapeutic Chemistry, School of Pharmacy and Food Sciences, University of Barcelona, 08028 Barcelona, Spain
[c] Department of Pharmacy and Pharmaceutical Technology and Physical, Chemistry. School of Pharmacy and Food Sciences, University of Barcelona, 08028 Barcelona, Spain
[d] Nanoscience and Nanotechnology Institute, IN2UB, University of Barcelona, Spain

ARTICLE INFO

Keywords:
PPRHs
DOPY
Cationic liposome
Gene delivery
Transfection
Gene silencing
Gene repair
Nucleic acids
Lipid-based vector
Cancer therapy

ABSTRACT

Nucleic acids therapeutics provide a selective and promising alternative to traditional treatments for multiple genetic diseases. A major obstacle is the development of safe and efficient delivery systems. Here, we report the synthesis of the new cationic gemini amphiphile 1,3-bis[(4-oleyl-1-pyridinio)methyl]benzene dibromide (DOPY). Its transfection efficiency was evaluated using PolyPurine Reverse Hoogsteen hairpins (PPRHs), a nucleic acid tool for gene silencing and gene repair developed in our laboratory. The interaction of DOPY with PPRHs was confirmed by gel retardation assays, and it forms complexes of 155 nm. We also demonstrated the prominent internalization of PPRHs using DOPY compared to other chemical vehicles in SH-SY5Y, PC-3 and DF42 cells. Regarding gene silencing, a specific PPRH against the *survivin* gene delivered with DOPY decreased survivin protein levels and cell viability more effectively than with *N*-[1-(2,3-Dioleoyloxy)propyl]-*N*,*N*,*N*-trimethylammonium methylsulfate (DOTAP) in both SH-SY5Y and PC-3 cells. We also validated the applicability of DOPY in gene repair approaches by correcting a point mutation in the endogenous *locus* of the *dhfr* gene in DF42 cells using repair-PPRHs. All these results indicate both an efficient entry and release of PPRHs at the intracellular level. Therefore, DOPY can be considered as a new lipid-based vehicle for the delivery of therapeutic oligonucleotides.

1. Introduction

The use of nucleic acids therapeutics has emerged as a promising gene therapy approach to modulate any gene of interest for the treatment of multiple diseases such as cancer [1,2] neurological [3-6], cardiovascular [7,8] or hematological [9,10] disorders, among others. The advances in this field have eventually led to the approval by the Food and Drug administration (FDA) of several nucleic acid tools [11], including antisense oligonucleotides (ASOs) [12-18], small interfering RNAs (siRNAs) [19-21], aptamers [22] or the very recent mRNA vaccines against COVID-19 [23,24].

Despite the great efforts made during the last decades, the development of safe, efficient and tissue-specific delivery systems still remains as one of the major limitations of gene therapies. In general, delivery vectors can be classified into viral, physical or chemical systems [25]. On the one hand, although viral vectors exhibit high transduction efficiencies, they can generate mutations in the DNA or undesired immunogenic responses. Moreover, the laborious production and the restriction on the transgene size also represent some of the limitations of viral vectors [26]. On the other hand, physical systems, which perturb the cell membrane to enforce the entry of nucleic acids into the cell, are safer but present lower efficiency than viral vectors and they are difficult to implement for internal organs [27]. Finally, chemical systems (e.g., calcium phosphate, lipoplexes or polyplexes) are safer than viral vectors,

* Corresponding authors at: School of Pharmacy and Food Sciences, University of Barcelona, 08028 Barcelona, Spain.
E-mail addresses: mlperez@ub.edu (L. Pérez-García), cciudad@ub.edu (C.J. Ciudad).
[1] Present address: Dipartimento di Medical Affairs, Novartis Farma, Via Saronnino 1, 21042, Origgio, Varese, Italy.
[2] Present address: Merck Serono Spa, Via Einaudi 11, 00012, Guidonia, Roma, Italy.

https://doi.org/10.1016/j.ejpb.2021.05.016
Received 22 February 2021; Received in revised form 15 April 2021; Accepted 18 May 2021
Available online 24 May 2021
0939-6411/© 2021 The Authors. Published by Elsevier B.V. This is an open access article under the CC BY license (http://creativecommons.org/licenses/by/4.0/).

easier to produce and susceptible to modifications to enhance targeting specificity. However, some of these chemical alternatives present low levels of internalization or some toxicity [28-30].

During the last decade, our laboratory of Biochemistry and Molecular biology has developed a new nucleic acid tool called PolyPurine Reverse Hoogsteen hairpins (PPRHs) [31,32]. PPRHs are non-modified DNA hairpins, whose structure is formed by two antiparallel polypurine mirror repeat domains linked by a five-thymidine loop (5T) and bound intramolecularly by Hoogsteen bonds. PPRHs are designed to hybridize to a specific polypyrimidine sequence in the dsDNA by Watson–Crick bonds, thus producing a triplex structure. This conformation displaces the fourth strand of the complex and leads to the inhibition of the target gene. The ability of PPRHs as gene silencing tools has been validated in a wide range of target genes involved in cancer progression both *in vitro* [33-42] and *in vivo* [35]. Furthermore, PPRHs have also demonstrated their potential to correct point mutations in the gDNA. The design of these PPRHs, called repair-PPRHs, consist of a polypurine hairpin that bears at its 5′-end an extension sequence homologous to the sequence to be repaired but containing the wild-type nucleotide instead of the mutated one [43,44]. Repair-PPRHs were able to correct at the endogenous level two collections of Chinese Hamster Ovary (CHO) cell lines bearing different mutations in either the *dihydrofolate reductase (dhfr)* [45] or *adenine phosphoribosyltransferase (aprt)* [46] *loci*.

As in other gene therapy methods, internalization of PPRHs is vital to obtain the desired effect. Regarding *in vitro* gene silencing approaches, we have routinely been delivering PPRHs in various cancer cell lines [35,36] using the *N*-[1-(2,3-Dioleoyloxy)propyl]-*N*,*N*,*N*-trimethylammonium methylsulfate (DOTAP) cationic liposome, which is commercially available [47,48]. However, the delivery of PPRHs in hard-to-transfect SH-SY5Y neuroblastoma cells was unsuccessful.

More than a decade ago our Organic Chemistry group created a new family of cationic gemini surfactants. The dicationic amphiphiles are formed by two cationic heterocycles -either imidazolium [49], pyridinium [50] or bipyridinium rings [51] linked by a 1,3-dimethylenephenylene spacer, where the cationic rings incorporate long alkyl chains of different lengths and functionality, their properties being driven by their specific structural composition. Over the years we have reported the ability of this class of amphiphiles to behave as ionic liquid crystals [52], their self-assembly into micelles as anion nanocarriers [53], as well as their use for the synthesis and stabilization of gold nanoparticles for drug delivery [54,55]. The bis cationic amphiphiles self-assemble to form nanostructured supramolecular hydrogels [56] for the topical treatment of Psoriasis and delivery in skin diseases [57,58] able to act as enhancers of skin permeation [59]. Both cationic amphiphilic incorporating nanoparticles [60] and hydrogels [61] have proven to be efficient deliverers of photosensitizers and their selective phototoxicity in cancer cells makes them promising nanomaterials for targeted photodynamic therapy [62].

The present work exemplifies the synergy created by the combination of the expertise of our two groups. Thus, with the aim to develop a non-viral vehicle capable of delivering PPRHs in hard-to-transfect cells, we designed and synthesized a new liposome formulation called 1,3-bis [(4-oleyl-1-pyridinio)methyl]benzene dibromide (DOPY) testing its capacity to form complexes with PPRH molecules. Due to its gemini cationic nature, the assemblies from DOPY are able to interact with polyanionic PPRH molecules, with the oleyl moieties aiding their cell uptake. In addition, we analyzed the efficiency of DOPY in gene silencing approaches by inhibiting the *survivin* gene in both PC3 and SH-SY5Y cancer cells using PPRHs. Finally, we validated DOPY as a transfection agent for gene repair applications by correcting a point mutation in the *dhfr* gene in CHO cells using repair-PPRHs.

2. Materials and methods

2.1. Chemicals and instrumentation

Oleyl alcohol, 4-chloropyridine hydrochloride, sodium hydride (NaH), α,α'-dibromo-m-xylene, dimethyl sulfoxide (DMSO), acetonitrile and deuterochloroform ($CDCl_3$) were purchased from Sigma-Aldrich. Ethyl acetate (AcOEt), hexane, sodium sulfate anhydrous (Na_2SO_4) and silica gel 60 were purchased from Carlo Erba. All chemicals were analytical grade and used directly without any further modification.

Evaporation of solvent was accomplished with a rotatory evaporator. Thin-layer chromatography was done on SiO_2 (silica gel 60 F254), and the spots were located by either an UV light or a 1% $KMnO_4$ solution. Flash column chromatography was carried out on SiO_2 (silica gel 60, 230–400 mesh).

NMR spectra were recorded at 400 MHz (^1H) and 100.6 MHz (^{13}C) on a Varian Mercury in the Scientific and Technologic Center of the University of Barcelona (CCiT-UB); chemical shifts are reported in δ values, in parts per million (ppm) relative to Me_4Si (0 ppm) or relative to residual chloroform (7.26 ppm, 77.00 ppm) as an internal standard. Data are reported in the following manner: chemical shift, multiplicity, coupling constant (*J*) in hertz (Hz), integrated intensity.

The hydrodynamic diameter of the liposomes was determined by dynamic light scattering (DLS) at a fixed scattering angle of 90° with a Zetasizer Nano (Malvern, United Kingdom) at 25 °C. To perform this measurement, lipoplexes were formed by mixing aqueous solutions of DOPY (2.1 uM) and PPRH against survivin (100 nM), mimicking the conditions of transfection. Nanoparticles were dissolved in 200 μL water and brought to 1 mL for the measurements. Particle size distribution was determined by the polydispersity index (PI). The ζ-potential was measured by Doppler microelectrophoresis using a Zetasizer Nano (Malvern, United Kingdom). For this measurement, the final volume of the lipoplexes was 1.2 mL.

Transmission Electron Microscopy (TEM) images were obtained in the CCiTUB. Samples of DOPY, PPRH, and DOPY-PPRH complexes were prepared in the same molar proportions used in transfection experiments. Copper grids with carbon coating were irradiated with a UV glow discharge during 30 s under vacuum. The grid was placed onto a 5 μL drop of the sample for 1 min. The grid was then placed onto a 20 μL drop of milli Q water for 1 min to rinse excess sample and then placed onto a 20 μL drop of a 2% uranyl acetate solution in water for 1 min. Excess solution was then removed with filter paper and allowed to dry overnight in a desiccator at 24 °C. Samples were observed in a Tecnai Spirit microscope (FEI, The Netherlands) equipped with a LaB6 cathode. Images were acquired at 120 kV and at room temperature with a 1376 × 1024-pixel Megaview CCD camera.

2.2. Preparation of 4-Oleyloxypyridine

Oleyl alcohol (1.3 mL, 4.09 mmol) was added dropwise to a stirring suspension of NaH (115 mg, 4.55 mmol, 95%) in dry DMSO (3 mL). After 45 min, crude 4-chloropyridine (800 mg, 7.05 mmol) (compound **1**, Fig. 1A), freshly liberated using KOH (2 N) from its hydrochloride salt, was added at once. The stirring was continued overnight at room temperature. Water was added and the mixture was extracted with AcOEt (3 × 10 mL), The combined organic extracts were dried over Na_2SO_4, filtered and concentrated at reduced pressure. Flash chromatography (from 3:2 to 1:1 hexane–EtOAc) afforded 4-oleyloxypyridine (510 mg, 50%) as a colourless oil. The structure of the 4-oleyloxypyridine (compound **2,** Fig. 1A) was characterized and confirmed by ^1H NMR and ^{13}C NMR spectroscopy (Figure S1).

^1H NMR (400 MHz, $CDCl_3$) δ: 8.39 (d, $J = 5.0$ Hz, 2H), 6.77 (d, $J = 5.0$ Hz, 2H), 5.30–5.38 (m, 2H), 3.98 (t, $J = 6.6$ Hz, 2H), 1.93–2.04 (m, 4H), 1.78 (quint, $J = 6.6$ Hz, 2H, H-6), 1.40–1.47 (m, 2H), 1.20–1.37 (m, 20H),0.87 (t, $J = 7.0$ Hz, 3H).

^{13}C NMR (100.6 MHz, $CDCl_3$) δ: 165.1, 150.9, 129.98, 129.7, 110.2,

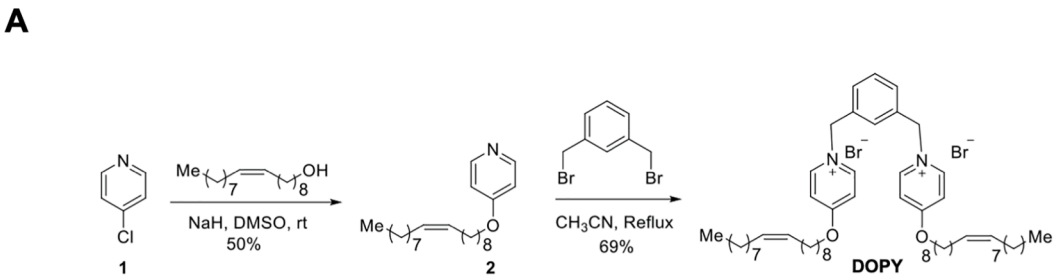

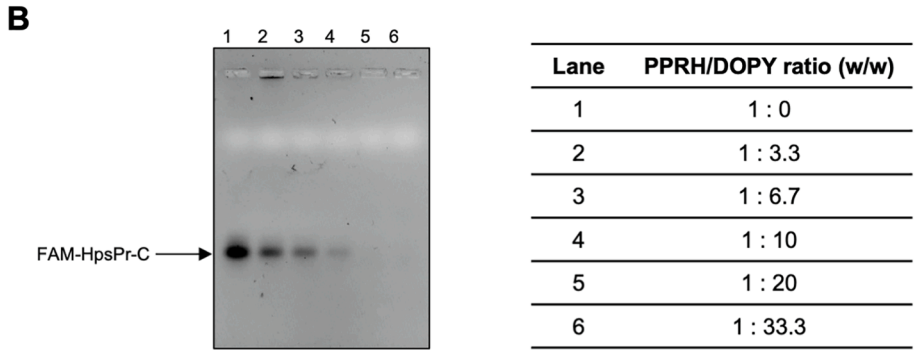

Lane	PPRH/DOPY ratio (w/w)
1	1 : 0
2	1 : 3.3
3	1 : 6.7
4	1 : 10
5	1 : 20
6	1 : 33.3

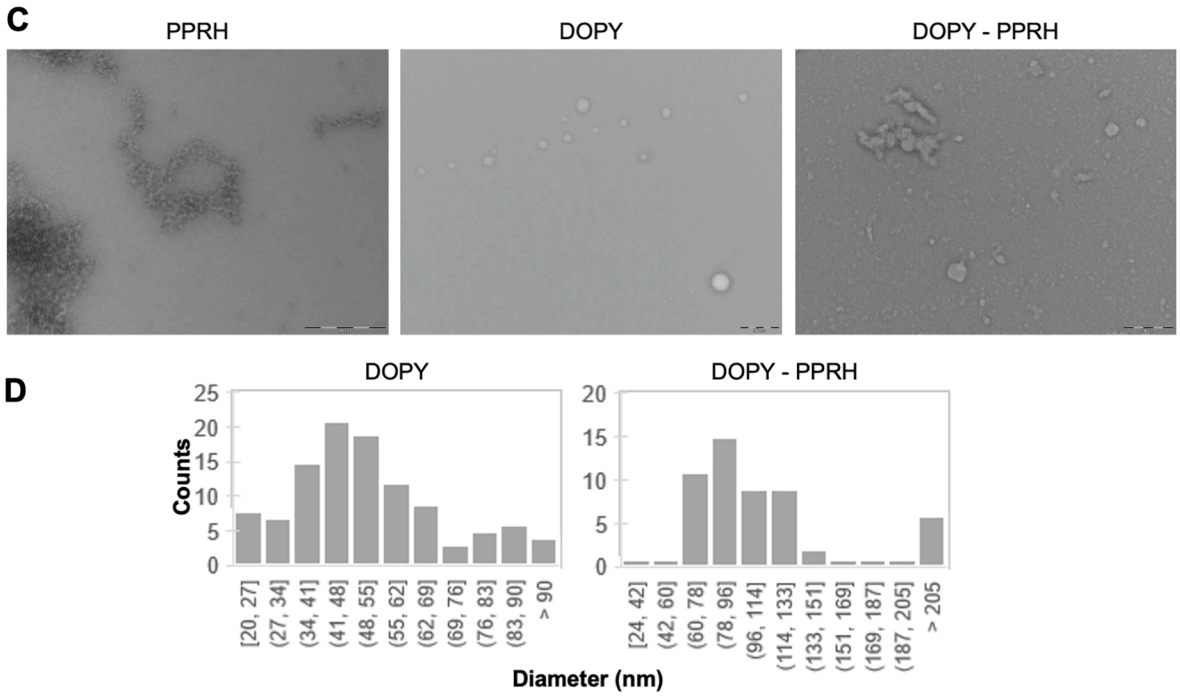

Fig. 1. DOPY synthesis and binding properties. (A) Schematic representation of the synthesis of 1,3-bis(4-olelyl-1-pyridiniomethyl)benzene dibromide (DOPY). Compounds **1** and **2** correspond to free pyridine and its oleyl ether, respectively. (B) Gel retardation assay with increasing amounts of DOPY, which binds to 150 ng of FAM-HpsPr-C and generates DOPY/PPRH complexes. C) TEM images of PPRH (left), DOPY (center), and DOPY-PPRH lipoplexes (right). D) Size distribution by half-open intervals of DOPY vesicles (left) (n = 109) and DOPY-PPRH lipoplexes (right) (n = 57) as observed by TEM.

67.9, 31.9, 29.7, 29.7, 29.5, 29.4, 29.3, 29.27, 29.2, 28.9, 27.2, 27.1 25.90, 22.7, 14.1.

2.3. Preparation of DOPY

α,α'-Dibromo-*m*-xylene (166 mg, 0.61 mmol) was added to a solution of 4-oleyloxypyridine (423 mg, 1.22 mmol) in acetonitrile (7 mL), and the mixture was heated at reflux for 24 h. After cooling at room temperature, the suspension was filtered off, and the resulting gum was washed with acetonitrile affording 1,3-bis(4-oleyloxy-1-pyridiniomethyl)benzene dibromide (DOPY) (400 mg, 69%, MW 956 g/mol), as a sticky yellowish solid (Fig. 1A). The structure of DOPY (Figure S2) was

characterized and confirmed by ^{1}H NMR and ^{13}C NMR spectroscopy.

^{1}H NMR (400 MHz, $CDCl_3$) δ 9.77 (d, $J = 7$ Hz, 4H), 8.36 (s, 1H), 7.69 (d, $J = 8$ Hz, 2H), 7.35 (d, $J = 7$ Hz, 4H), 7.00 (t, $J = 8$ Hz, 1H), 5.94 (s, 4H), 5.39–5.30 (m, 4H), 4.21 (t, $J = 6$ Hz, 4H), 2.05–1.94 (m, 8H), 1.84 (quint, $J = 7$ Hz, 4H), 1.47–1.39 (m, 4H), 1.38–1.22 (m, 40H), 0.87 (t, $J = 7$ Hz, 6H).

^{13}C NMR (100.6 MHz, $CDCl_3$) δ: 170.0, 146.3, 134.5, 130.7, 129.9, 129.6, 129.3, 113.8, 71.2, 60.9, 32.2, 31.5, 29.4, 29.3, 29.2, 29.1, 29.0, 28.9, 28.8, 28.7, 28.1, 26.8, 26.7, 26.7, 25.3, 22.3.

2.4. Design and usage of PPRHs

For gene silencing experiments, a PPRH directed against the *survivin* promoter previously validated in our laboratory was selected [35,63]. The polypurine stretches that conform the hairpin structure of the PPRH were found using the Triplex-forming Oligonucleotide Target Sequence Search software (http://utw10685.utweb.utexas.edu/tfo/ MD Anderson cancer center, The University of Texas) [64]. BLAST analyses were performed to confirm the specificity of the designed PPRH. As negative control, we used a hairpin with intramolecular Watson–Crick bonds instead of Hoogsteen bonds (HpWC), thus preventing triplex formation with the target DNA.

Regarding the gene repair approach, repair-PPRHs were designed by attaching an extension sequence (repair domain) at the 5′-end of the PPRH. This repair domain is homologous to the mutation site but containing the corrected nucleotide instead. As negative control, a scrambled repair-PPRH was used. This negative repair-PPRH contained the specific repair domain to correct the mutation but a scrambled polypurine hairpin core, which cannot bind to the polypyrimidine target sequence near the mutation in the dsDNA.

All hairpins were synthesized as non-modified oligodeoxynucleotides by Merck (Haverhill, United Kingdom), resuspended in sterile Tris-EDTA buffer (1 mM EDTA and 10 mM Tris, pH 8.0) (Merck, Madrid, Spain) and stored at −20 °C until use. All the sequences of the hairpins used in this study are shown in Table 1.

2.5. Agarose gel retardation assay

Binding reactions were conducted in a final volume of 10 μL containing 150 ng of FAM-HpsPr-C PPRH, increasing amounts of DOPY and H_2O mQ. After 20 min of incubation at room temperature, binding reactions were electrophoresed in 0.8% agarose gels. Gels were visualized on a Gel Doc™ EZ (Bio-Rad Laboratories, Inc, Spain).

2.6. Cell culture

For gene silencing experiments, SH-SY5Y neuroblastoma and PC-3 prostate cancer cells, obtained from the cell bank resources from University of Barcelona, were grown in Ham's F12 medium supplemented with 10% fetal bovine serum (GIBCO, Invitrogen, Barcelona, Spain) and incubated at 37 °C in a humidified 5% CO_2 atmosphere. Subculture was performed using 0.05% Trypsin (Merck, Madrid, Spain).

For gene correction experiments, the DF42 Chinese Hamster Ovary (CHO) mutant cell line was used. This cell line contained a single-point mutation in the endogenous *dhfr* gene bearing a G > T substitution in c.541 (exon 6), thus generating a premature STOP codon and a nonfunctional DHFR enzyme. The DF42 cell line was obtained using a variety of mutagens in UA21 cells [65], which is a CHO cell line hemizygous for the *dhfr* gene [66]. Cells were grown as stated previously.

2.7. Transfection of PPRHs

Regarding gene silencing experiments, cells were plated in 6-well dishes one day before transfection in F12 medium. Transfection

Table 1
Oligodeoxynucleotides used in this study.

Name	Sequence (5'-3')
FAM-HpsPr-C	[6FAM] AGGGGAGGGATGGAGTGCAG T T T AGGGGAGGGATGGAGTGCAG T T
HpsPr-C	AGGGGAGGGATGGAGTGCAG T T T AGGGGAGGGATGGAGTGCAG T T
HpWC	GACGTGAGGTAGGGAGGGGA T T T AGGGGAGGGATGGAGTGCAG T T
HpE6rep-L	GAAGTCCAGGAGGAAAAAGGCATCAAGTATAAATTT**G**AAGTCTATGAGAAGAAAGGCTAACAGAAAGA T T T GAGAAGAAAGGCTAACAGAAAGA T T
HpE6rep-L-Sc	GAAGTCCAGGAGGAAAAAGGCATCAAGTATAAATTT**G**AAGTCTATAGAGGAGGGAATCGGTGAGGGAG T T T AGAGGAGGGAATCGGTGAGGGAG T T

Name and sequence of the PPRHs used for gel retardation and cellular uptake assays (FAM-HpsPr-C), gene silencing experiments (HpsPr-C and the negative control HpWC) and gene repair approaches (HpE6rep-L and the negative control HpE6rep-L-Sc). The corrected nucleotide in the repair-PPRHs is represented in bold and underlined. The abbreviations used for the nomenclature of the PPRHs are: Hp, hairpin; Pr, promoter; s, survivin; -C, Coding-PPRH; -WC, Watson:Crick; E6, exon 6; rep, repair- PPRH; Sc, scramble.

consisted in mixing the corresponding amount of the transfection agent with the PPRH in serum-free medium up to 200 μL. After 20 min of incubation at room temperature, the mixture was added to the cells in a final volume of 1 mL (full medium). Transfection agents used were the newly synthesized compound DOPY or the commercially available cationic liposome DOTAP (Biontex, Germany).

For gene correction experiments, DF42 cells (300,000) were plated in 100-mm plates the day before transfection. Transfections were performed using either calcium phosphate, DOTAP or DOPY. Calcium phosphate transfections were carried out using the original method [67], and similarly to our previous works [43,45,46]. DOTAP transfections were performed by mixing 12 μg of DOTAP with 10 μg of repair-PPRH in serum-free medium up to 600 μL. After 20 min of incubation, DOTAP/repair-PPRH complexes were added to cells in a final volume of 6 mL (full medium) (Final concentration of DOTAP 2.6 μM). DOPY transfections were performed by mixing 12 μg of DOPY with 10 μg of repair-PPRH in serum-free medium up to 600 μL. After 20 min of incubation, DOPY/repair-PPRH complexes were added to cells in a final volume of 6 mL (full medium) (Final concentration of DOPY 2.1 μM). In all types of transfections, cells were incubated during 48 h with repair-PPRHs before selection.

2.8. Cellular uptake

SH-SY5Y cells (60,000), PC-3 cells (60,000) or DF42 cells (300,000) were plated the day before transfection. Transfections were carried out as stated previously in the transfection section of M&M, but in this case using FAM-HpsPr-C PPRH. After 24 h of incubation, cell images for each condition were taken using a ZOE Fluorescent Cell Imager (Bio-Rad Laboratories, Inc, Spain). Then, cells were trypsinized and collected, centrifuged at 800*g* at 4 °C for 5 min and washed once in PBS. The pellet was resuspended in 500 μL of PBS and Propidium Iodide was added to a final concentration of 5 μg/mL (Merck, Madrid, Spain). Flow cytometry analyses were performed in a Gallios flow cytometer (Beckman Coulter, Inc, Spain).

To study the internalization mechanism of DOPY, SH-SY5Y and PC-3 cells (120,000) were plated in 6-well dishes in F12 medium. After 24 h, cells were preincubated with 75 μM of the clathrin-dependent endocytosis inhibitor Dynasore [68], 185 μM of the caveolin-mediated endocytosis inhibitor Genistein [69], or 33 μM of the micropinocytosis inhibitor 5-(*N*-ethyl-*N*-isopropyl) amiloride (EIPA) [70], all from Merck, Madrid, Spain, for 60 min at 37 °C. Then, transfection mixes containing FAM-HpsPr-C were added to cells for 4 h and processed for flow cytometry analyses as described above in this section.

2.9. MTT assay

Cells (10,000) were plated in 6-well dishes in F12 medium. Five (PC-3 cells) or four (SH-SY5Y cells) days after transfection, 0.63 mM of 3-(4,5- dimetilthyazol-2-yl)-2,5-dipheniltetrazolium bromide and 100 μM sodium succinate (both from Merck, Madrid, Spain) were added to the culture medium and incubated for 2.5 h at 37 °C. After incubation, culture medium was removed and the lysis solution (0.57% of acetic acid and 10% of sodium dodecyl sulfate (SDS) in dimethyl sulfoxide) (Merck, Madrid, Spain) was added. Absorbance was measured at 560 nm in a Modulus Microplate spectrophotometer (Turner BioSystems, Madrid, Spain). Cell viability results were expressed as the percentage of cell survival relative to the controls.

2.10. Western blot analyses

Total protein extracts from PC-3 and SH-SY5Y cells (30,000) were obtained 24 h after transfection using 100 μL of RIPA buffer (1% Igepal, 0.5% sodium deoxycholate, 0.1% SDS, 150 mM NaCl, 1 mM EDTA, 1 mM PMSF, 10 mM NaF and 50 mM Tris-HCl, pH 8.0) supplemented with Protease inhibitor cocktail (P8340) (all from Merck, Madrid, Spain). Extracts were incubated 5 min at 4 °C and cell debris was removed by centrifugation (16,300*g* at 4 °C for 10 min).

In the case of DF42 protein extracts, cells were harvested by trypsinization and treated with Lysis buffer (0.5 M NaCl, 1.5 mM $MgCl_2$, 1 mM EDTA, 10% glycerol, 1% Triton X-100, 50 mM HEPES, pH 7.2), supplemented with Protease Inhibitor Mixture (P8340) (all from Merck, Madrid, Spain). Whole-protein extracts were maintained at 4 °C for 1 h with vortexing every 15 min. Cell debris was removed by centrifugation (16,300*g* for 10 min).

Protein concentrations were determined using a Bio-Rad protein assay based on the Bradford method and using bovine serum albumin as a standard. Whole-protein extracts (100 μg) were electrophoresed in 15% or 12% SDS-polyacrylamide gels for survivin or DHFR detection, respectively, and transferred to Immobilon-P polyvinylidene difluoride membranes (Merck, Madrid, Spain) using a semidry electroblotting system. Blocking was performed using a 5% skim milk solution. Then, membranes were probed with the primary antibody against survivin (5 μg/mL; AF886, Bio-Techne R&D Systems, S.L.U. Madrid, Spain), DHFR (1:250 dilution; Pocono Rabbit Farm & Lab, Canadensis, PA, USA) or α-Tubulin (1:100 dilution; CP06, Merck, Darmstadt, Germany. Secondary horseradish peroxidase-conjugated antibodies were anti-rabbit (1:2000 dilution; P0399, Dako, Denmark) for primary antibodies against survivin and DHFR, and anti-mouse (1:2500 dilution; sc-516102, Santa Cruz Biotechnology, Heidelberg, Germany) for α-tubulin detection. Chemiluminescence was detected with the ImageQuant LAS 4000 mini (GE Healthcare, Barcelona, Spain). Quantification was performed using the ImageQuant 5.2 software.

2.11. Selection of repaired cells

DHFR selection was applied to transfected cells after 48 h of incubation with the repair-PPRH. Selection was performed using RPMI 1640 selective medium (Gibco) lacking glycine, hypoxanthine and thymidine (-GHT medium), which are the final products of DHFR activity, and containing 7% dialyzed FBS (Gibco). Each experimental condition was performed in triplicate, and a minimum of three colonies were analyzed for each condition.

2.12. Gene correction frequency

After 14 days of selection in -GHT medium, surviving cell colonies were fixed in 6% formaldehyde, stained with crystal violet (both from Merck, Madrid, Spain) and manually counted. Gene correction frequency values were calculated as the ratio between the number of surviving colonies and the total number of cells initially plated.

2.13. DNA sequencing

Total genomic DNA was isolated from either DF42 mutant or DF42 repaired cells using the Wizard genomic DNA purification kit (Promega, Madrid, Spain) following the manufacturer's recommendations. PCRs were carried out to amplify the target site using OneTaq polymerase (New England Biolabs, Ipswich, MA, USA) following the PCR cycling conditions recommended by the manufacturer. Primer sequences were 5′-GTCATGTGTCTTCAATGGGTG-3′ and 5′-TCTAAAGCCAACACAAGTCCC-3′. PCR-amplified products (227 bp) were run in 5% polyacrylamide gel electrophoresis, purified and sequenced by Macrogen (Amsterdam, the Netherlands).

2.14. DHFR activity assay

The method is based on the incorporation of radioactive deoxyuridine into cellular DNA. This depends on the reductive methylation of deoxyuridylate to thymidylate by tetrahydrofolate, which is generated by DHFR from folate supplied in the medium. Therefore, incorporation of radioactive dTTP into DNA relies on DHFR activity, and it can be

detected by DNA isolation [71].

Mutant or repaired DF42 cells (1×10^5) were seeded in 6-well plates in 1 mL of selective medium (-GHT). Next day, 2 μCi of 6-[^{3}H] deoxyuridine (18.9 Ci/mmol, Hartmann Analytic, Germany) were added for 24 h. Cells were lysed in 100 μL of 0.1% SDS. The lysate was placed onto 31ET chromatography paper (Whatman) and dried at room temperature. Finally, papers were washed three times for 30 min in constant agitation with 66% cold ethanol containing 250 mM NaCl, dried, and counted in a scintillation counter.

2.15. Statistical analyses

Statistical analyses were performed using GraphPad Prism 6 (GraphPad Software, CA, USA). Data are represented as the mean ± SEM

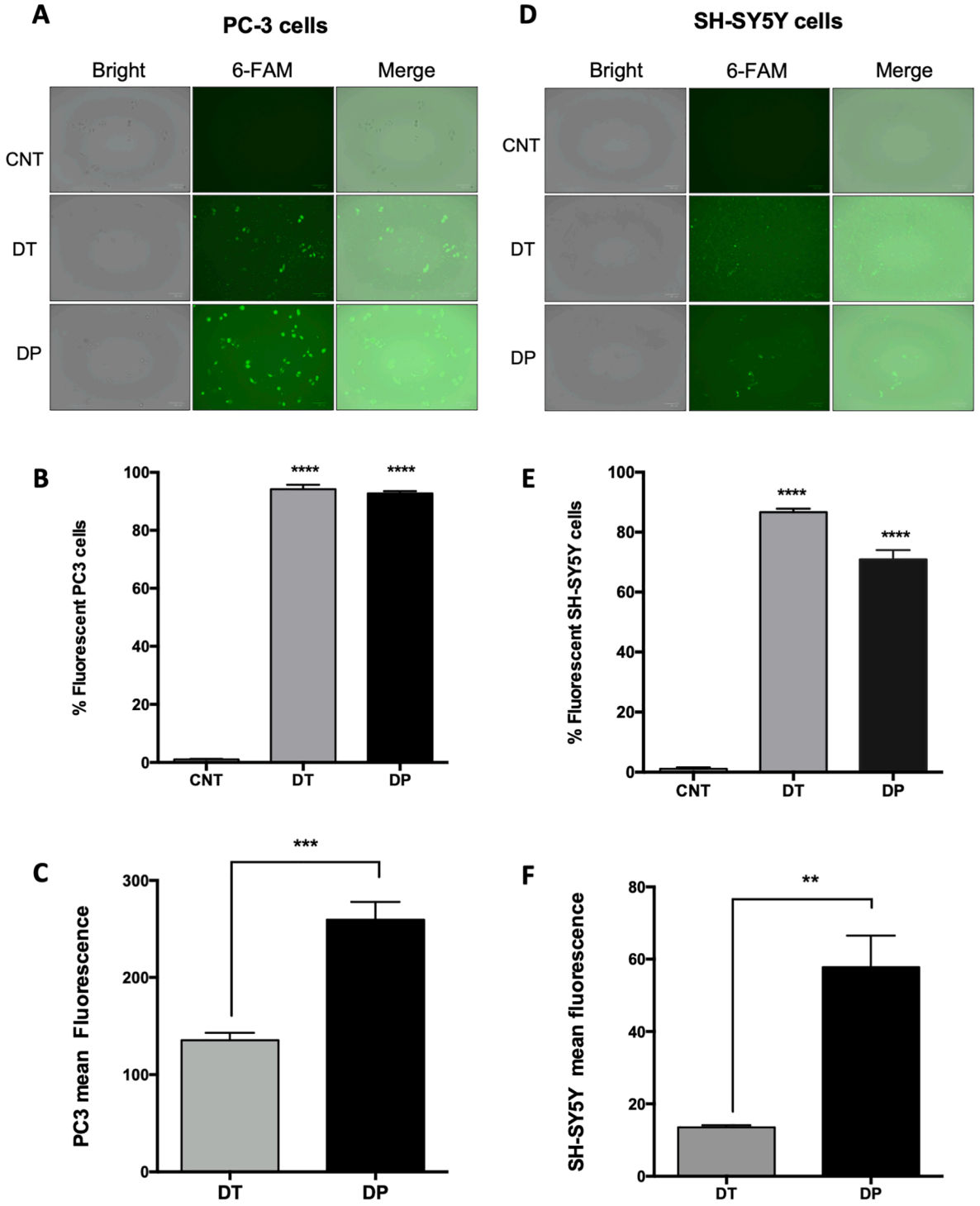

Fig. 2. Cellular uptake of PPRHs for gene silencing applications. Fluorescence microscopy images of PC-3 (A) and SH-SY5Y (D) cells were taken 24 h after transfection with 100 nM of FAM-HpsPr-C using either DOTAP (10 μM) or DOPY (2.1 μM). Then, the percentage of fluorescent cells (B and E) and the mean fluorescence (C and F) for each cell line were determined by flow cytometry. Error bars represent the standard error of the mean of three experiments. Statistical significance was calculated using one-way ANOVA with Dunnett's multiple comparisons test for the percentage fluorescent cells or Unpaired T test for the mean fluorescence (**$p < 0.01$, ***$p < 0.001$, **** $p < 0.0001$). Abbreviations: CNT, control; DT, DOTAP; DP, DOPY.

of at least three independent experiments. The levels of statistical significance were denoted as follows: $p < 0.05$ (*), $p < 0.01$ (**), $p < 0.001$ (***) or $p < 0.0001$ (****).

3. Results

3.1. DOPY/PPRH complexes characterization

First, the ability of DOPY to interact with FAM-HpsPr-C PPRH was assessed by gel retardation assays. Incubation of increasing amounts of DOPY with 150 ng of the PPRH resulted in a progressive disappearance of the band corresponding to the PPRH signal compared to the PPRH alone (Fig. 1B), thus demonstrating the formation of DOPY/PPRH complexes. Then, we analyzed the size of DOPY/PPRH complexes, which show an hydrodynamic diameter of 155 nm, with a dispersion index of 0.25 (Figure S3A), as analyzed by DLS, a value significantly increased respect the DOPY vesicles (*ca.* 100 nm) upon complexation. Furthermore, the Z-potential of DOPY/PPRH complexes 67.53 ± 1.08 mV (Figure S3B), is not significantly different from that of DOPY vesicles (*ca.* 57 mV), in accordance with the cationic nature of the lipoplexes, and indicates the excellent stability of the lipoplexes.

Transmission Electron Microscopy (TEM) was used to study the morphology of the materials. As shown in Fig. 1C, the FAM-HpsPr-C PPRH molecules intertwine forming fibrillar structures, whereas DOPY forms vesicles of 52.4 ± 18.2 nm in diameter (Fig. 1D). In contrast, when DOPY vesicles come in contact with PPRH, the fibers of PPRH are completely covered by DOPY as a consequence of their strong interaction, leading to a combined morphology. Most of the lipoplexes formed are less than 133 nm in diameter (Fig. 1D), which is also in accordance with the hydrodynamic diameters observed in aqueous colloidal dispersion.

3.2. Transfection efficiency for gene silencing

Once verified the capacity of DOPY to interact with PPRHs, we compared the cellular uptake of FAM-HpsPr-C PPRH (100 nM) when cells were transfected using either DOPY or the validated transfection agent DOTAP, which is widely used in our laboratory for gene silencing approaches, and thus useful for comparison purposes in the different assays. Cells were transfected using either 2.1 μM of DOPY or 10 μM of DOTAP (standard conditions used for PPRH transfection in gene silencing approaches: molar ratio of 1:100 PPRH/DOTAP). The percentage of fluorescent cells and their mean fluorescence intensity were determined 24 h after transfection using flow cytometry. The cellular uptake was analyzed in PC-3 cells, in which we had previous experience transfecting PPRHs using DOTAP, and in SH-SY5Y cells, which are difficult to transfect using DOTAP in standardized conditions. According to our previous results using HpsPr-C PPRH [35], high percentages of fluorescent PC-3 cells were observed when using DOTAP (94%) (Fig. 2A and B). Similar values of fluorescent cell percentages were obtained when using DOPY (93%) (Fig. 2B). However, the mean values were 2-fold higher in DOPY transfections than those of DOTAP (Fig. 2C). In the case of hard-to-transfect SH-SY5Y cells, the percentages of fluorescent cells were 87% using DOTAP and 71% using DOPY (Fig. 2D and E), but the fluorescence mean was 4.3 times higher in DOPY transfections than that of DOTAP transfections (Fig. 2F). Fluorescence microscopy cell images acquired just before flow cytometer analyses were in accordance with the results described in this section (Fig. 2A and D).

We also analyzed the mechanisms involved in the internalization of DOPY/PPRH complexes by transfecting cells with FAM-HpsPr-C either in the presence or the absence of different endocytic pathways inhibitors (Fig. 3) [68-70]. After 4 h of transfection, DOPY/PPRH complexes internalization was significatively reduced with either the clathrin-dependent endocytosis inhibitor Dynasore (75 μM) or the caveolin-mediated endocytosis inhibitor Genistein (185 μM), in both PC-3 and SH-SY5Y cells. The treatment with Dynasore presented a decrease of 51% and 35% of fluorescent cells, in PC-3 and SH-SY5Y respectively, in comparison with untreated cells (Fig. 3A and C). Furthermore, the fluorescence mean values were reduced by 24.5 and 3.4-fold in PC-3 and SH-SY5Y cells, respectively, relative to untreated cells (Fig. 3B and D). In the case of Genistein treatment, the decrease of fluorescent cells was of 23% in PC-3 and 21% in SH-SY5Y (Fig. 3A and C), and the fluorescence mean values were reduced by 20-fold and 2.7-fold in PC-3 and SH-SY5Y cells, respectively (Fig. 3B and D). No significant decrease was observed in neither the percentage of fluorescent cells nor the fluorescent mean in neither of the two cell lines treated with the micropinocytosis inhibitor EIPA (33 μM) (Fig. 3). These results indicate that both the clathrin-mediated endocytosis and the caveolin-mediated endocytosis are involved in DOPY/PPRH complexes internalization. Fluorescence microscopy cell images are shown in Figure S4.

3.3. Cell viability assays

Previous work in our laboratory demonstrated that the inhibition of the antiapoptotic gene *survivin* using PPRHs led to a decrease in prostate cancer cell survival both *in vitro* and *in vivo* [33,35]. Therefore, we used PC-3 cells as a positive control since we had evidence of the effectiveness of transfecting the HpsPr-C PPRH using DOTAP in this type of cells [35]. In this work, we searched for a non-toxic amount of DOPY for each cell line. The optimum concentration in PC-3 cells was ranging from 0.52 −1.05 μM (Fig. 4A), whereas SH-SY5Y cells could be incubated with higher doses of DOPY (1.05–2.1 μM) (Fig. 4B). Then, 100 nM of HpsPr-C PPRH was transfected using either DOTAP or DOPY to compare the effect on cell viability caused by the PPRH. PC-3 cells transfected with DOTAP/HpsPr-C complexes showed a decrease in cell viability of 90% (Fig. 4A). Similarly, cells transfected using 0.52 μM and 1.05 μM of DOPY showed a reduction in cell viability of 97% and 99%, respectively (Fig. 4A).

However, in the case of SH-SY5Y cells, incubations with DOTAP/HpsPr-C complexes at standard conditions did not reduce cell viability, whereas cells treated with DOPY/HpsPr-C complexes showed a decrease in cell viability of 36% and 84% using 1.05 μM and 2.1 μM of DOPY, respectively (Fig. 4B). Transfections with the negative control hairpin (HpWC) did not produce any effect on cell viability in PC-3 and SH-SY5Y cells (Fig. 4A and B).

3.4. Survivin protein analyses

To confirm that the detrimental effect on cell viability was caused by a specific decrease of *survivin* expression triggered by 100 nM of HpsPr-C PPRH, we analyzed survivin protein levels in both PC-3 and SH-SY5Y cells. After 24 h of incubation, PC-3 cells transfected using either DOTAP (10 μM) or DOPY (1,05 μM) presented a 75% reduction on survivin protein levels (Fig. 5A). In contrast, SH-SY5Y cells transfected with DOTAP (10 μM) did not show a significant decrease in protein expression (Fig. 5B), while cells transfected using DOPY (2.1 μM) showed a decrease of 85% on survivin protein levels.

3.5. Transfection efficiency for gene repair

One of the goals of this work was to demonstrate the versatility of transfection of DOPY. For that reason, we also used DOPY for gene correction applications. In this regard, repair-PPRHs were delivered into the DF42 CHO mutant cell line to correct a point mutation in the endogenous *locus* of the *dhfr* gene. The HpE6rep-L repair-PPRH was designed to correct the c.541 G > T mutation in this gene (Table 1). HpE6rep-L consisted in (i) a 23 nt polypurine core complementary to its polypyrimidine target sequence located 9 nt downstream from the mutation, and (ii) a 45 nt repair domain homologous to the mutation region but containing the desired nucleotide (G) instead of the mutation (T).

First, the delivery of PPRHs into DF42 cells was assessed by fluorescence microscopy (Fig. 6A) and flow cytometry (Fig. 6B and C) using

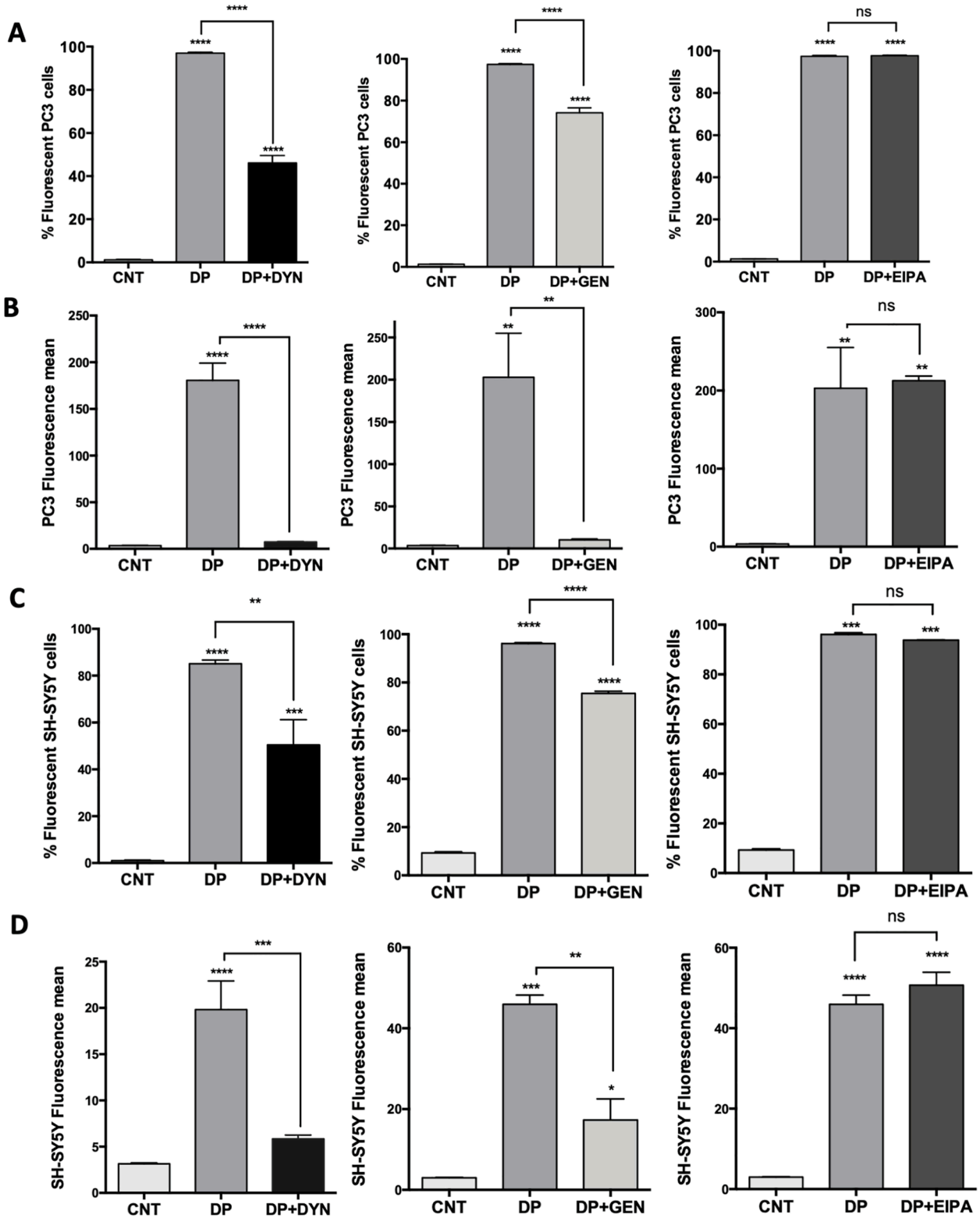

Fig. 3. Study of the endocytic pathways involved in DOPY/PPRH complexes internalization. PC-3 and SH-SY5Y cells were incubated for 1 h with 75 μM of Dynasore, 185 μM Genistein, or 33 μM EIPA and subsequently transfected with 100 nM of the FAM-HpsPr-C PPRH using 2.1 μM of DOPY. After 4 h of incubation, the percentage of fluorescent cells (A and C) and the mean fluorescence (B and D) for each cell line were determined by flow cytometry. Error bars represent the standard error of the mean of three experiments. Statistical significance was calculated using one-way ANOVA with Tukey's multiple comparisons test for the percentage fluorescent cells and the mean fluorescence (*$p < 0.05$, **$p < 0.01$, ***$p < 0.001$, **** $p < 0.0001$). Abbreviations: CNT, control; DP, DOPY; DYN, Dynasore; GEN, Genistein; EIPA, 5-(*N*-ethyl-*N*-isopropyl)amiloride; ns, not statistically significant.

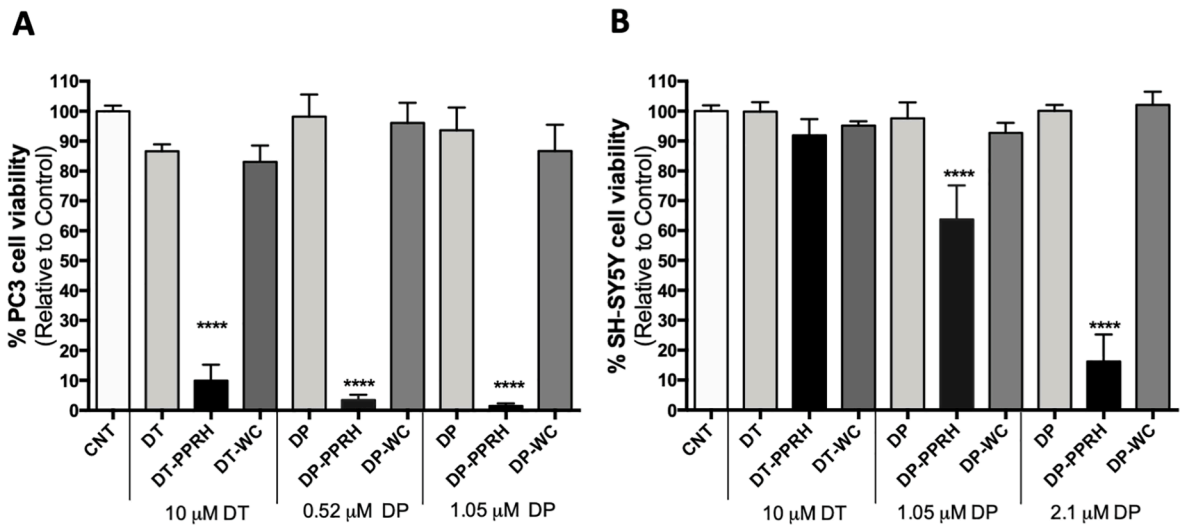

Fig. 4. Effect of HpsPr-C on cell viability in PC-3 and SH-SY5Y cells. Effect on cell viability in PC-3 (A) and SH-SY5Y (B) upon transfection of 100 nM the HpsPr-C PPRH or the negative control hairpin (HpWC) using DOTAP (DT) or DOPY (DP). The concentrations for each transfection agent are indicated in the figure. Error bars represent the standard error of the mean of three experiments. Statistical significance was calculated using one-way ANOVA with Dunnett's multiple comparisons test (**** $p < 0.0001$).

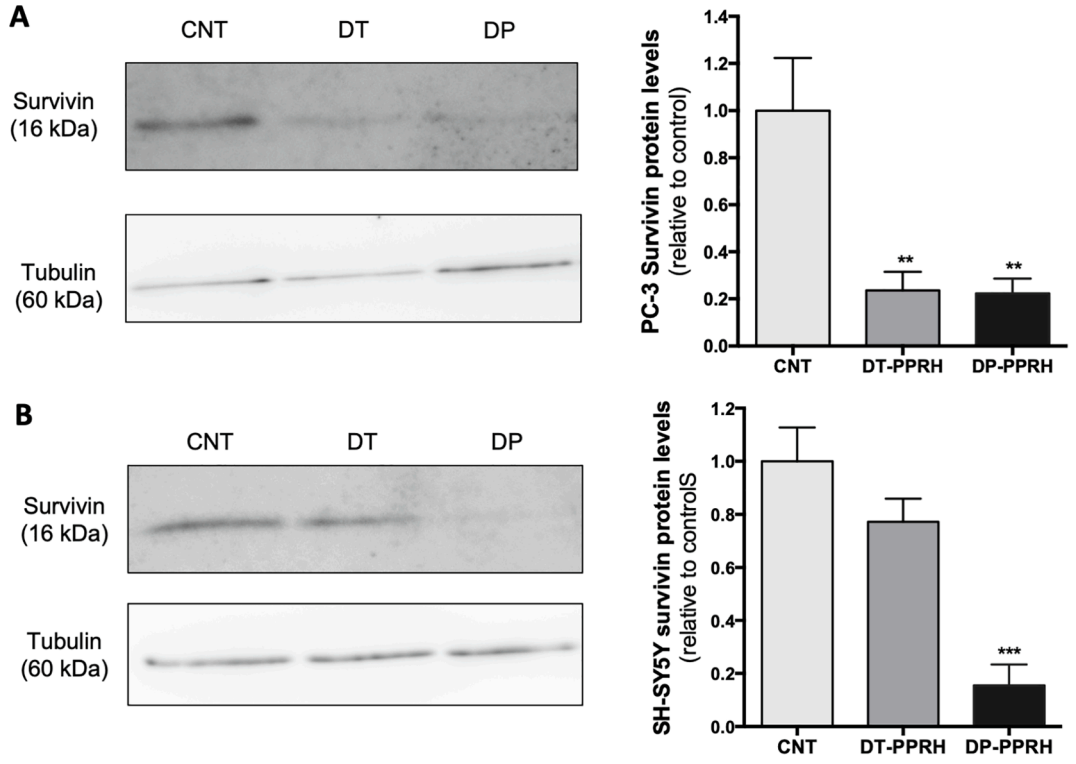

Fig. 5. Comparison of the effect of HpsPr-C on survivin protein levels using either DOTAP or DOPY as transfection agent. PC-3 (A) and SH-SY5Y (B) cells were transfected with 100 nM of the HpsPr-C PPRH using either DOTAP (10 μM) or DOPY (1.05 μM for PC-3 cells and 2.1 μM for SH-SY5Y cells) and incubated for 24 h. Representative images of Western blots (left) and quantification of survivin protein levels relative to the control (right) are shown. Tubulin protein levels were used to normalize the results. Error bars represent the standard error of the mean of three experiments. Statistical significance was calculated using one-way ANOVA with Dunnett's multiple comparisons test (**$p < 0.01$, ***$p < 0.001$). Abbreviations: CNT, control; DT, DOTAP; DP, DOPY.

FAM-HpsPr-C PPRH. The efficiency of transfection of DOPY in DF42 cells was compared to that of calcium phosphate or DOTAP, since both methodologies are standardly used in our laboratory for the delivery of repair-PPRHs. Both DOTAP and DOPY transfections were able to deliver PPRHs to more than 80% of the total cell population, whereas calcium phosphate transfections only achieved 50% of transfection efficiency (Fig. 6B). However, mean fluorescence values showed that the highest internalization was obtained using DOPY (Fig. 6C). It is worth noting that calcium phosphate transfections presented lower internalization values than those of DOPY, but higher than those of DOTAP (Fig. 6C). Fluorescence microscopy cell images acquired just before flow cytometer analyses were in accordance with the results described in this section (Fig. 6A).

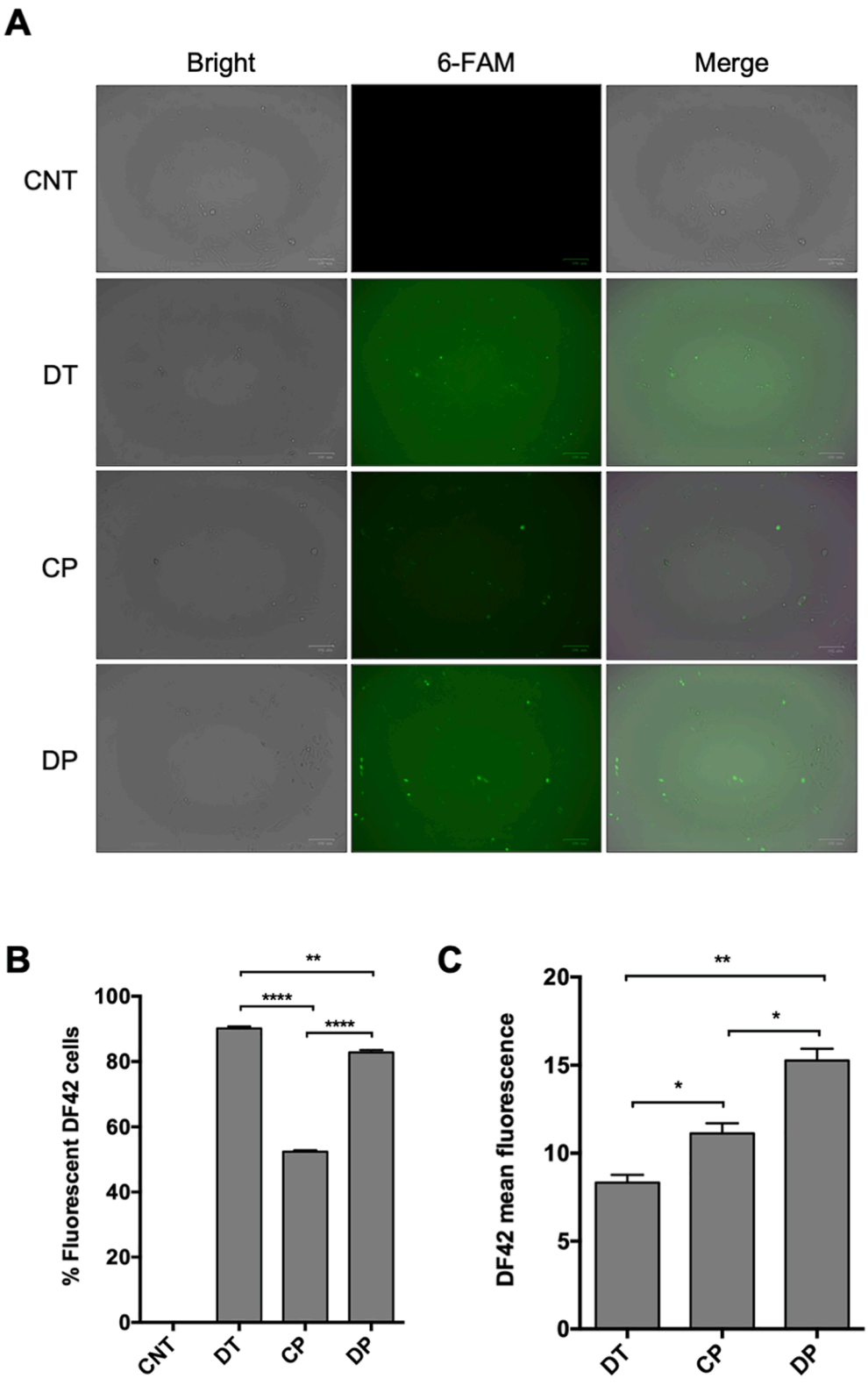

Fig. 6. Cellular uptake of PPRHs for gene repair applications. (A) DF42 cells were transfected with 10 μg of FAM-HpsPr-C (112 nM) using DOTAP (2.6 μM), calcium phosphate or DOPY (2.1 μM) and visualized under a fluorescence microscope after 24 h of incubation. Then, cells were harvested and analyzed by flow cytometry to determine the (B) percentage of DF42 fluorescent cells and (C) the mean fluorescence. Error bars represent the standard error of the mean of three experiments. Statistical significance was calculated using Unpaired T test comparing the effect of the different transfection agents (*$p < 0.05$, **$p < 0.01$, **** $p < 0.0001$). Abbreviations: CNT, control; DT, DOTAP; CP, calcium phosphate; DP, DOPY.

3.6. Gene correction frequency

After 48 h of incubation with repair-PPRHs, selective medium (-GHT) was applied during 14 days. At this point, cell colonies were stained and counted to determine gene repair frequencies for each transfection method. In these experimental conditions, no cell colonies were obtained when transfecting using DOTAP (Fig. 7A). However, calcium phosphate transfections generated a 0.2% of corrected cells, while DOPY transfections led to repair frequencies of 0.4%, which represented a 2-fold increase compared to calcium phosphate frequencies (Fig. 7B).

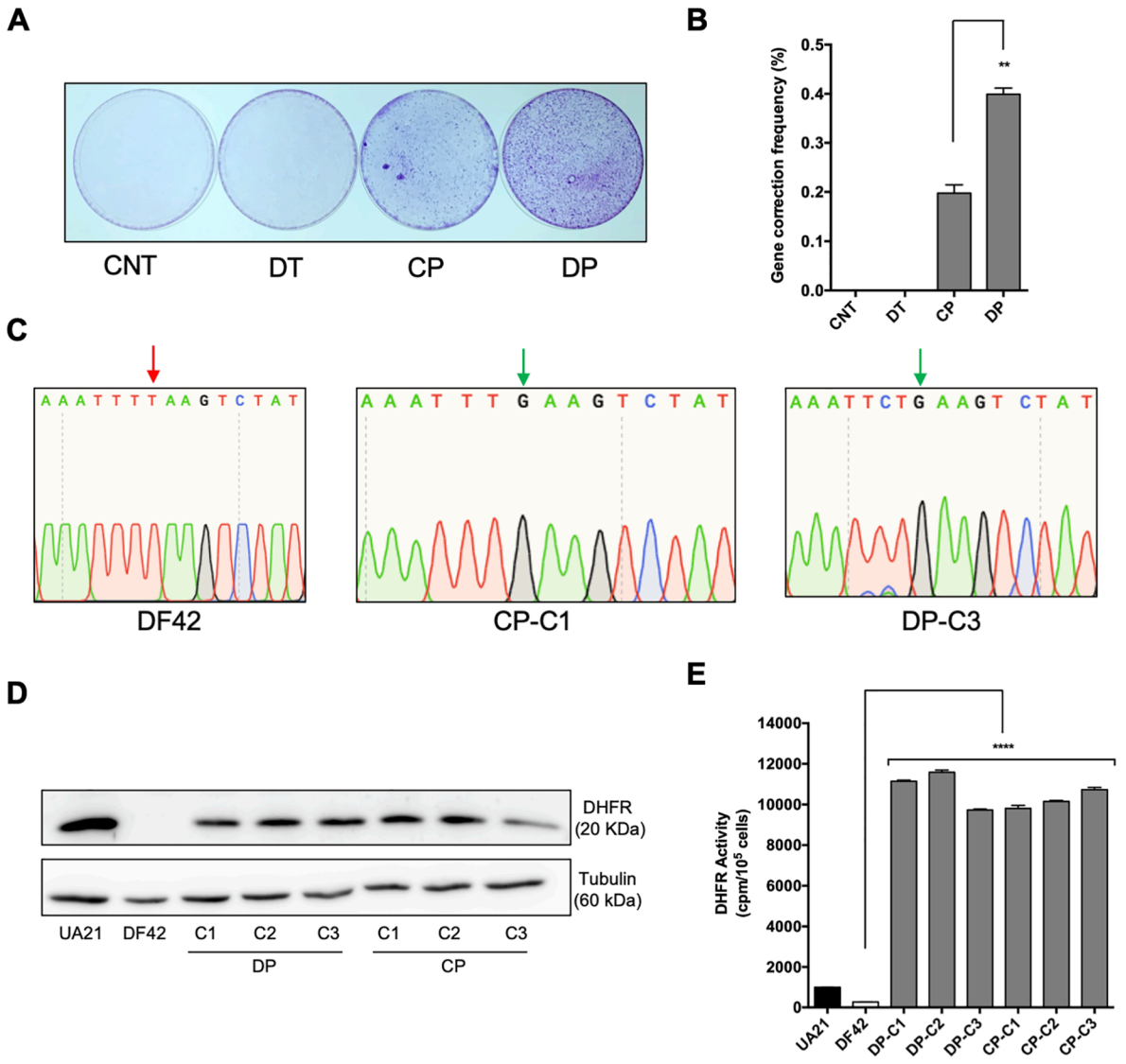

Fig. 7. Gene correction frequency and characterization of DF42 repaired clones. (A) Representative image of the number of DF42 repaired colonies obtained after transfection with 10 μg of the HpE6rep-L repair-PPRH (55 nM) using DOTAP (2.6 μM), calcium phosphate or DOPY (2.1 μM). After selection, surviving cell colonies were fixed and stained with crystal violet. (B) Gene correction frequency values were calculated as the ratio between the number of DF42 surviving colonies and the total number of cells initially plated. (C) DNA sequences from DF42 mutant and DF42 repaired cells after treatment with the HpE6rep-L repair-PPRH using calcium phosphate or DOPY are shown. Red and green arrows indicate the mutated and corrected nucleotide, respectively. (D) Western blotting of DHFR protein in DF42 mutant cells and DF42 repaired clones. Tubulin protein was used as endogenous control. (E) DHFR enzymatic activity was determined in DF42 mutant cells and DF42 repaired clones. UA21 parental cells were used as positive control. Error bars represent the standard error of the mean of three experiments. Statistical significance was calculated using Unpaired T test in (B) and ordinary one-way ANOVA in (E). (**$p < 0.01$, **** $p < 0.0001$). Abbreviations: CNT, control; DT, DOTAP; CP, calcium phosphate; DP, DOPY.

3.7. Characterization of dhfr repaired clones

After selection, a representative number of cell colonies from each transfection condition were expanded individually and analyzed at the DNA level to confirm the correction of the mutation. As shown in Fig. 7C, both calcium phosphate and DOPY transfections of the HpE6rep-L repair-PPRH were able to correct the c.541 G > T mutation at the genomic level in DF42 cells, thus restoring the wild-type sequence of the *dhfr* gene.

In addition, we corroborated that the restoration of the wild type *dhfr* sequence in the DNA of the repaired clones led to the production of DHFR protein. Western blot assays showed the presence of DHFR protein in all the analyzed clones derived from both calcium phosphate and DOPY transfections (Fig. 7D). DHFR protein was also present in the wild-type UA21 cell line, used as positive control (Fig. 7D).

Finally, we demonstrated the functionality of the DHFR protein by determining its enzymatic activity. All the repaired clones derived from both calcium phosphate and DOPY transfections showed a similar enzymatic activity, which represented a 50-fold increase compared to that of mutant DF42 cells (Fig. 7E).

4. Discussion

In this work, we describe DOPY as a new gemini cationic liposome-based formulation for PPRH delivery and evaluate its transfection efficiency for both gene silencing and gene repair applications. We chose PPRH delivery since these molecules represent an economical biotechnological tool with advantages compared to other therapeutic oligonucleotides [31,32]. PPRHs are more stable than siRNAs due to its clamp structure composed of deoxynucleotides instead of ribonucleotides [72].

Furthermore, PPRHs are effective at lower concentrations than ASOs [33] and they bind with higher affinity to the target dsDNA than Triplex-Forming Oligonucleotides (TFOs) [37]. In terms of safety, PPRHs have demonstrated their lack of immunogenicity [72], nephrotoxicity and hepatotoxicity *in vitro* [63]. Moreover, pharmacogenomic studies demonstrated the specificity of PPRHs and the absence of off-target effects [63].

It is known that cationic lipid-based delivery systems form electrostatic complexes with DNA. This condensation protects DNA from nuclease degradation and confers desirable physicochemical properties in terms of size and charge to facilitate DNA entry into cells [73]. In several chemical vectors, the positive charge is provided by a pyridinium salt [74-76]. Following this approach, in the present work we designed DOPY, a gemini amphiphilic bis-pyridinium salt connected through a 1,3-xylyl spacer and bearing hydrophobic oleyl moieties on the position 4 of the pyridinium rings, to study its ability as DNA carrier. In solution, these complexes have *ca.* 155 nm in diameter, as determined by DLS. Accordingly, gel retardation assays demonstrated that DOPY can form complexes with PPRHs, thus pairing their negative charges. Transmission Electron Microscopy experiments also corroborate this interaction and allows the visualization of the fibrillar structures of the PPRH molecules covered by DOPY.

To achieve the desired effect of PPRHs within the cell, a successful transfection requires their internalization into the cytoplasm and their transportation into the nucleus. Regarding PPRHs internalization, DOPY has demonstrated high delivery efficiencies in PC-3, SH-SY5Y and DF42 cells. Interestingly, the amount of PPRH internalized by DOPY complexes was higher than that of other chemical vehicles routinely used in our laboratory such as DOTAP or calcium phosphate. These higher values of internalization can explain the superior effects obtained in both gene silencing and gene repair approaches using PPRHs compared to that of other transfection agents. Additionally, the decrease in DOPY/PPRH cellular uptake after Dynasore or Genistein treatment in both PC-3 and SH-SY5Y cells suggests that the clathrin-mediated endocytosis and the caveolae-dependent endocytosis are involved in the internalization of PPRHs mediated by DOPY.

In gene silencing experiments, we targeted the antiapoptotic gene survivin, which has been correlated with different types of cancer such as prostate [77], breast [78], gastric [79,80], osteosarcoma [81] or neuroblastoma [82,83]. Since we faced difficulties in transfecting neuroblastoma SH-SY5Y cells with commercially available agents, we transfected the HpsPr-C PPRH directed against survivin in SH-SY5Y cells using DOPY. DOPY/HpsPr-C complexes successfully decreased survivin protein levels and cell viability in hard-to-transfect SH-SY5Y cells, even using nearly 4-fold less amount of DOPY than that of DOTAP. These results are in accordance with other studies showing the inhibition of SH-SY5Y cell proliferation due to an increase of apoptosis after suppressing survivin expression [84]. In contrast, the transfection of DOTAP/HpsPr-C complexes in SH-SY5Y cells did not reduce survivin protein levels nor cell viability, which corroborates the greater internalization capacity of DOPY. In the case of PC-3 cells, our previous studies transfecting HpsPr-C using DOTAP showed an effective delivery and survivin gene silencing [35]. In this work, we showed a great reduction on protein levels and cell viability using 7.75-fold less amount of DOPY than that of DOTAP. Therefore, DOPY/PPRH complexes are more effective in terms of inhibiting survivin expression and reducing cell viability in both SH-SY5Y and PC-3 cells.

In gene correction experiments, the HpE6rep-L repair-PPRH transfected using DOPY in DF42 mutant cells achieved higher correction frequencies than that of DOTAP or calcium phosphate transfection agents, which are the chemical vehicles routinely used in our laboratory for gene correction strategies [45,46]. The HpE6rep-L repair-PPRH was able to specifically correct the c.541 G > T mutation in the endogenous locus of the dhfr gene, thus restoring its wild-type sequence. In addition, we confirmed that DF42 corrected cells were able to produce a full DHFR protein with restored enzymatic activity, thus proving the effectivity of DOPY as a transfection agent also in gene repair approaches.

Overall, the successful cellular uptake, the efficient survivin gene silencing and the correction of the dhfr gene are evidence that DOPY enables both an efficient entry and release of PPRHs at the intracellular level, thus allowing them to exert their action in the target dsDNA. Although further studies to demonstrate safety and efficacy of DOPY *in vitro* and *in vivo* should be performed, the results to date indicate that DOPY can be considered as a new gemini cationic lipid-based delivery vector suitable for the delivery of therapeutic oligonucleotides.

Declaration of Competing Interest

The authors declare that they have no known competing financial interests or personal relationships that could have appeared to influence the work reported in this paper.

Acknowledgements

This research was funded by grant RTI2018-093901-B-I00 from MICINN (Spain), by EU ERDF (FEDER) funds and the Spanish Government grant TEC2017-85059-C3-2-R, and by *Ajut a la Recerca Transversal 2018* from IN2UB, and the Serra Hunter programme (RG). Groups holding the Quality Mention from Generalitat de Catalunya 2017-SGR-94 and 2017-SGR-1277. AJF and EA are awarded with fellowships from Ministerio de Educación (FPU) and Generalitat de Catalunya (FI), respectively, and CS and CM obtained fellowships from the Erasmus program.

Appendix A. Supplementary data

Supplementary data to this article can be found online at https://doi.org/10.1016/j.ejpb.2021.05.016.

References

[1] M.H. Amer, Gene therapy for cancer: present status and future perspective, Mol. Cell. Ther. 2 (2014) 27, https://doi.org/10.1186/2052-8426-2-27.
[2] S.M. Parsel, J.R. Grandis, S.M. Thomas, Nucleic acid targeting: Towards personalized therapy for head and neck cancer, Oncogene. 35 (2016) 3217–3226, https://doi.org/10.1038/onc.2015.424.
[3] T.T. Nielsen, J.E. Nielsen, Antisense gene silencing: Therapy for neurodegenerative disorders? Genes (Basel). 4 (2013) 457–484, https://doi.org/10.3390/genes4030457.
[4] E.A. Burton, J.C. Glorioso, D.J. Fink, Gene therapy progress and prospects: Parkinson's disease, Gene Ther. 10 (2003) 1721–1727, https://doi.org/10.1038/sj.gt.3302116.
[5] J.M. Alisky, B.L. Davidson, Gene therapy for amyotrophic lateral sclerosis and other motor neuron diseases, Hum. Gene Ther. 11 (2000) 2315–2329, https://doi.org/10.1089/104303400750038435.
[6] A.M. Winkelsas, K.H. Fischbeck, Nucleic acid therapeutics in neurodevelopmental disease, Curr. Opin. Genet. Dev. 65 (2020) 112–116, https://doi.org/10.1016/j.gde.2020.05.022.
[7] E.G. Nabel, Gene therapy for cardiovascular diseases, J. Nucl. Cardiol. 6 (1999) 69–75, https://doi.org/10.1016/S1071-3581(99)90066-1.
[8] U. Landmesser, W. Poller, S. Tsimikas, P. Most, F. Paneni, T.F. Lü Scher, From traditional pharmacological towards nucleic acid-based therapies for cardiovascular diseases, Eur. Heart J. 41 (2020) 3884–3899, https://doi.org/10.1093/eurheartj/ehaa229.
[9] C.E. Walsh, Gene therapy progress and prospects: Gene therapy for the hemophilias, Gene Ther. 10 (2003) 999–1003, https://doi.org/10.1038/sj.gt.3302024.
[10] I. Hazan-Halevy, D. Landesman-Milo, D. Rosenblum, S. Mizrahy, B.D. Ng, D. Peer, Immunomodulation of hematological malignancies using oligonucleotides based-nanomedicines, J. Control. Release. 244 (2016) 149–156, https://doi.org/10.1016/j.jconrel.2016.07.052.
[11] T.C. Roberts, R. Langer, M.J.A. Wood, Advances in oligonucleotide drug delivery, Nat. Rev. Drug Discov. 19 (2020) 673–694, https://doi.org/10.1038/s41573-020-0075-7.
[12] FDA News Release, FDA grants accelerated approval to first targeted treatment for rare Duchenne muscular dystrophy mutation | FDA, FDA. (2019). https://www.fda.gov/news-events/press-announcements/fda-grants-accelerated-approval-first-targeted-treatment-rare-duchenne-muscular-dystrophy-mutation (accessed January 18, 2021).
[13] IONIS press release, Akcea and Ionis Receive FDA Approval of TEGSEDITM (inotersen) for the Treatment of the Polyneuropathy of Hereditary Transthyretin-

Mediated Amyloidosis in Adults | Ionis Pharmaceuticals, Inc., IONIS. (2018). https://ir.ionispharma.com/news-releases/news-release-details/akcea-and-ionis-receive-fda-approval-tegseditm-inotersen (accessed January 18, 2021).
[14] FDA News Release, FDA approves first drug for spinal muscular atrophy | FDA, FDA. (2016). https://www.fda.gov/news-events/press-announcements/fda-approves-first-drug-spinal-muscular-atrophy (accessed January 18, 2021).
[15] FDA News Release, FDA grants accelerated approval to first drug for Duchenne muscular dystrophy | FDA, FDA. (2016). https://www.fda.gov/news-events/press-announcements/fda-grants-accelerated-approval-first-drug-duchenne-muscular-dystrophy (accessed January 18, 2021).
[16] FDA News Release, FDA approves first treatment for rare disease in patients who receive stem cell transplant from blood or bone marrow, FDA. (2016). https://www.fda.gov/NewsEvents/Newsroom/PressAnnouncements/ucm493225.htm (accessed January 18, 2021).
[17] P. Hair, F. Cameron, K. McKeage, Mipomersen sodium: First global approval, Drugs. 73 (2013) 487–493, https://doi.org/10.1007/s40265-013-0042-2.
[18] L. Highleyman, FDA approves fomivirsen, famciclovir, and Thalidomide. Food and Drug Administration - PubMed, BETA. (1998). https://pubmed.ncbi.nlm.nih.gov/11365993/ (accessed January 18, 2021).
[19] D. Adams, A. Gonzalez-Duarte, W.D. O'Riordan, C.C. Yang, M. Ueda, A.V. Kristen, I. Tournev, H.H. Schmidt, T. Coelho, J.L. Berk, K.P. Lin, G. Vita, S. Attarian, V. Planté-Bordeneuve, M.M. Mezei, J.M. Campistol, J. Buades, T.H. Brannagan, B. J. Kim, J. Oh, Y. Parman, Y. Sekijima, P.N. Hawkins, S.D. Solomon, M. Polydefkis, P.J. Dyck, P.J. Gandhi, S. Goyal, J. Chen, A.L. Strahs, S.V. Nochur, M.T. Sweetser, P.P. Garg, A.K. Vaishnaw, J.A. Gollob, O.B. Suhr, Patisiran, an RNAi therapeutic, for hereditary transthyretin amyloidosis, N. Engl. J. Med. 379 (2018) 11–21, https://doi.org/10.1056/NEJMoa1716153.
[20] L.J. Scott, Givosiran: First Approval, Drugs. 80 (2020) 335–339, https://doi.org/10.1007/s40265-020-01269-0.
[21] FDA News Release, FDA Approves First Drug to Treat Rare Metabolic Disorder | FDA, FDA. (2020). https://www.fda.gov/news-events/press-announcements/fda-approves-first-drug-treat-rare-metabolic-disorder (accessed December 9, 2020).
[22] S.A. Doggrell, Pegaptanib: The first antiangiogenic agent approved for neovascular macular degeneration, Expert Opin. Pharmacother. 6 (2005) 1421–1423, https://doi.org/10.1517/14656566.6.8.1421.
[23] FDA News Release, Pfizer-BioNTech COVID-19 Vaccine | FDA, FDA. (2020). https://www.fda.gov/emergency-preparedness-and-response/coronavirus-disease-2019-covid-19/pfizer-biontech-covid-19-vaccine (accessed January 7, 2021).
[24] FDA News Release, Moderna COVID-19 Vaccine | FDA, FDA. (2020). https://www.fda.gov/emergency-preparedness-and-response/coronavirus-disease-2019-covid-19/moderna-covid-19-vaccine (accessed January 7, 2021).
[25] N. Nayerossadat, P. Ali, T. Maedeh, Viral and nonviral delivery systems for gene delivery, Adv. Biomed. Res. 1 (2012) 27, https://doi.org/10.4103/2277-9175.98152.
[26] N. Slade, Viral vectors in gene therapy, Period. Biol. 103 (2001) 139–143, https://doi.org/10.3390/diseases6020042.
[27] M. Alsaggar, D. Liu, Physical Methods for Gene Transfer, Adv. Genet. 89 (2015) 1–24, https://doi.org/10.1016/bs.adgen.2014.10.001.
[28] D.W. Pack, A.S. Hoffman, S. Pun, P.S. Stayton, Design and development of polymers for gene delivery, Nat. Rev. Drug Discov. 4 (2005) 581–593, https://doi.org/10.1038/nrd1775.
[29] M.C. Filion, N.C. Phillips, Major limitations in the use of cationic liposomes for DNA delivery, Int. J. Pharm. 162 (1998) 159–170, https://doi.org/10.1016/s0378-5173(97)00423-7.
[30] B.I. Florea, C. Meaney, H.E. Junginger, G. Borchard, Transfection efficiency and toxicity of polyethylenimine in differentiated Calu-3 and nondifferentiated COS-1 cell cultures, AAPS PharmSci. 4 (2002) 1, https://doi.org/10.1208/ps040312.
[31] C.J. Ciudad, L. Rodríguez, X. Villalobos, A.J. Félix, V. Noé, Polypurine Reverse Hoogsteen Hairpins as a Gene Silencing Tool for Cancer, Curr. Med. Chem. 24 (2017), https://doi.org/10.2174/0929867324666170301114127.
[32] V. Noé, E. Aubets, A.J. Félix, C.J. Ciudad, Nucleic acids therapeutics using PolyPurine Reverse Hoogsteen hairpins, Biochem. Pharmacol. (2020) 114371. https://doi.org/10.1016/j.bcp.2020.114371.
[33] M.C. de Almagro, S. Coma, V. Noé, C.J. Ciudad, Polypurine hairpins directed against the template strand of DNA knock down the expression of mammalian genes, J. Biol. Chem. 284 (2009) 11579–11589, https://doi.org/10.1074/jbc.M900981200.
[34] M.C. De Almagro, N. Mencia, V. Noé, C.J. Ciudad, Coding polypurine hairpins cause target-induced cell death in breast cancer cells, Hum. Gene Ther. 22 (2011) 451–463, https://doi.org/10.1089/hum.2010.102.
[35] L. Rodríguez, X. Villalobos, S. Dakhel, L. Padilla, R. Hervas, J.L. Hernández, C. J. Ciudad, V. Noé, Polypurine reverse Hoogsteen hairpins as a gene therapy tool against survivin in human prostate cancer PC3 cells in vitro and in vivo, Biochem. Pharmacol. 86 (2013) 1541–1554, https://doi.org/10.1016/j.bcp.2013.09.013.
[36] X. Villalobos, L. Rodríguez, A. Solé, C. Lliberós, N. Mencia, C.J. Ciudad, V. Noé, Effect of polypurine reverse hoogsteen hairpins on relevant cancer target genes in different human cell lines, Nucleic Acid Ther. 25 (2015) 198–208, https://doi.org/10.1089/nat.2015.0531.
[37] L. Rodríguez, X. Villalobos, A. Solé, C. Lliberós, C.J. Ciudad, V. Noé, Improved design of PPRHs for gene silencing, Mol. Pharm. 12 (2015) 867–877, https://doi.org/10.1021/mp5007008.
[38] G. Bener, A.J. Félix, C. Sánchez de Diego, I. Pascual Fabregat, C.J. Ciudad, V. Noé, Silencing of CD47 and SIRPα by Polypurine reverse Hoogsteen hairpins to promote MCF-7 breast cancer cells death by PMA-differentiated THP-1 cells, BMC Immunol. 17 (2016) 1–12, https://doi.org/10.1186/s12865-016-0170-z.
[39] M.M.M. Enríquez, A.J. Félix, C.J. Ciudad, V. Noé, Cancer immunotherapy using PolyPurine Reverse Hoogsteen hairpins targeting the PD-1/PD-L1 pathway in human tumor cells, PLoS One. 13 (2018), https://doi.org/10.1371/journal.pone.0206818.
[40] C.J. Ciudad, M.M.M. Enriquez, A.J. Félix, G. Bener, V. Noé, Silencing PD-1 and PD-L1: The potential of PolyPurine Reverse Hoogsteen hairpins for the elimination of tumor cells, Immunotherapy. 11 (2019) 369–372, https://doi.org/10.2217/imt-2018-0215.
[41] E. Aubets, V. Noé, C.J. Ciudad, Targeting replication stress response using polypurine reverse hoogsteen hairpins directed against WEE1 and CHK1 genes in human cancer cells, Biochem. Pharmacol. 175 (2020), https://doi.org/10.1016/j.bcp.2020.113911.
[42] E. Aubets, A.J. Félix, M. Garavís, L. Reyes, A. Aviñó, R. Eritja, C.J. Ciudad, V. Noé, Detection of a g-quadruplex as a regulatory element in thymidylate synthase for gene silencing using polypurine reverse hoogsteen hairpins, Int. J. Mol. Sci. 21 (2020) 1–22, https://doi.org/10.3390/ijms21145028.
[43] A. Solé, X. Villalobos, C.J. Ciudad, V. Noé, Repair of single-point mutations by polypurine reverse hoogsteen hairpins, Hum. Gene Ther. Methods. 25 (2014) 288–302, https://doi.org/10.1089/hgtb.2014.049.
[44] A.J. Félix, A. Solé, V. Noé, C.J. Ciudad, Gene Correction of Point Mutations Using PolyPurine Reverse Hoogsteen Hairpins Technology, Front. Genome Ed. 2 (2020), 583577, https://doi.org/10.3389/fgeed.2020.583577.
[45] A. Solé, C.J. Ciudad, L.A. Chasin, V. Noé, Correction of point mutations at the endogenous locus of the dihydrofolate reductase gene using repair-PolyPurine Reverse Hoogsteen hairpins in mammalian cells, Biochem. Pharmacol. 110–111 (2016) 16–24, https://doi.org/10.1016/j.bcp.2016.04.002.
[46] A.J. Félix, C.J. Ciudad, V. Noé, Correction of the aprt Gene Using Repair-Polypurine Reverse Hoogsteen Hairpins in Mammalian Cells, Mol. Ther. - Nucleic Acids. 19 (2020) 683–695, https://doi.org/10.1016/j.omtn.2019.12.015.
[47] S. Falsini, S. Ristori, Lipoplexes from non-viral cationic vectors: DOTAP-DOPE liposomes and gemini micelles, in: Methods Mol. Biol., Humana Press Inc., 2016: pp. 33–43. https://doi.org/10.1007/978-1-4939-3718-9_3.
[48] R. Leventis, J.R. Silvius, Interactions of mammalian cells with lipid dispersions containing novel metabolizable cationic amphiphiles, BBA - Biomembr. (1990), https://doi.org/10.1016/0005-2736(90)90017-I.
[49] C. Sporer, L. Casal, D. Caballero, J. Samitier, A. Errachid, L. Pérez-García, Novel anionophores for biosensor applications: nano characterisation of SAMS based on amphiphilic imidazolium protophanes and cyclophanes on gold surfaces, Sens. Lett. 7 (2009) 757–764, https://doi.org/10.1166/sl.2009.1144.
[50] M.E. Alea-Reyes, A. González, A.C. Calpena, D. Ramos-López, J. de Lapuente, L. Pérez-García, Gemini pyridinium amphiphiles for the synthesis and stabilization of gold nanoparticles for drug delivery, J. Colloid Interface Sci. 502 (2017) 172–183, https://doi.org/10.1016/j.jcis.2017.04.064.
[51] S. Giraldo, M.E. Alea-Reyes, D. Limón, A. González, M. Duch, J.A. Plaza, D. Ramos-López, J. de Lapuente, A. González-Campo, L. Pérez-García, π-Donor/π-Acceptor interactions for the encapsulation of neurotransmitters on functionalized polysilicon-based microparticles, Pharmaceutics. 12 (2020) 1–19, https://doi.org/10.3390/pharmaceutics12080724.
[52] L. Casal-Dujat, O. Penon, C. Rodríguez-Abreu, C. Solans, L. Pérez-García, Macrocyclic ionic liquid crystals, New J. Chem. 36 (2012) 558–561, https://doi.org/10.1039/c2nj20934a.
[53] L. Casal-Dujat, P.C. Griffiths, C. Rodríguez-Abreu, C. Solans, S. Rogers, L. Pérez-García, Nanocarriers from dicationic bis-imidazolium amphiphiles and their interaction with anionic drugs, J. Mater. Chem. B. 1 (2013) 4963–4971, https://doi.org/10.1039/c3tb20289e.
[54] L. Casal-Dujat, M. Rodrigues, A. Yagüe, A.C. Calpena, D.B. Amabilino, J. Gonzaílez-Linares, M. Borraís, L. Peírez-Garciía, Gemini imidazolium amphiphiles for the synthesis, stabilization, and drug delivery from gold nanoparticles, Langmuir. 28 (2012) 2368–2381, https://doi.org/10.1021/la203601n.
[55] M. Rodrigues, A.C. Calpena, D.B. Amabilino, D. Ramos-López, J. De Lapuente, L. Pérez-García, Water-soluble gold nanoparticles based on imidazolium gemini amphiphiles incorporating piroxicam, RSC Adv. 4 (2014) 9279–9287, https://doi.org/10.1039/c3ra44578j.
[56] M. Samperi, L. Pérez-García, D.B. Amabilino, Quantification of energy of activation to supramolecular nanofibre formation reveals enthalpic and entropic effects and morphological consequence, Chem. Sci. 10 (2019) 10256–10266, https://doi.org/10.1039/c9sc03280k.
[57] M. Rodrigues, A.C. Calpena, D.B. Amabilino, M.L. Garduño-Ramírez, L. Pérez-García, Supramolecular gels based on a gemini imidazolium amphiphile as molecular material for drug delivery, J. Mater. Chem. B. 2 (2014) 5419–5429, https://doi.org/10.1039/c4tb00450g.
[58] D. Limón, C. Jiménez-Newman, A.C. Calpena, A. González-Campo, D.B. Amabilino, L. Pérez-García, Microscale coiling in bis-imidazolium supramolecular hydrogel fibres induced by the release of a cationic serine protease inhibitor, Chem. Commun. 53 (2017) 4509–4512, https://doi.org/10.1039/c6cc09392b.
[59] N.J. Starr, K. Abdul Hamid, J. Wibawa, I. Marlow, M. Bell, L. Pérez-García, D. A. Barrett, D.J. Scurr, Enhanced vitamin C skin permeation from supramolecular hydrogels, illustrated using in situ ToF-SIMS 3D chemical profiling, Int. J. Pharm. 563 (2019) 21–29, https://doi.org/10.1016/j.ijpharm.2019.03.028.
[60] M.E. Alea-Reyes, J. Soriano, I. Mora-Espí, M. Rodrigues, D.A. Russell, L. Barrios, L. Pérez-García, Amphiphilic gemini pyridinium-mediated incorporation of Zn(II) meso-tetrakis(4-carboxyphenyl)porphyrin into water-soluble gold nanoparticles for photodynamic therapy, Colloids Surfaces B Biointerfaces. 158 (2017) 602–609, https://doi.org/10.1016/j.colsurfb.2017.07.033.
[61] M. Samperi, D. Limón, D.B. Amabilino, L. Pérez-García, Enhancing Singlet Oxygen Generation by Self-Assembly of a Porphyrin Entrapped in Supramolecular Fibers,

Cell Reports Phys. Sci. 1 (2020), 100030, https://doi.org/10.1016/j.xcrp.2020.100030.
[62] O. Penon, M.J. Marín, D.A. Russell, L. Pérez-García, Water soluble, multifunctional antibody-porphyrin gold nanoparticles for targeted photodynamic therapy, J. Colloid Interface Sci. 496 (2017) 100–110, https://doi.org/10.1016/j.jcis.2017.02.006.
[63] A.J. Félix, C.J. Ciudad, V. Noé, Functional pharmacogenomics and toxicity of PolyPurine Reverse Hoogsteen hairpins directed against survivin in human cells, Biochem. Pharmacol. 155 (2018) 8–20, https://doi.org/10.1016/j.bcp.2018.06.020.
[64] S.S. Gaddis, Q. Wu, H.D. Thames, J. Digiovanni, E.F. Walborg, M.C. Macleod, K. M. Vasquez, A web-based search engine for triplex-forming oligonucleotide target sequences, Oligonucleotides. 16 (2006) 196–201, https://doi.org/10.1089/oli.2006.16.196.
[65] A.M. Carothers, G. Urlaub, R.W. Steigerwalt, L.A. Chasin, D. Grunberger, Characterization of mutations induced by 2-(N-acetoxy-N-acetyl)aminofluorene in the dihydrofolate reductase gene of cultured hamster cells, Proc. Natl. Acad. Sci. USA 83 (1986) 6519–6523, https://doi.org/10.1073/pnas.83.17.6519.
[66] G. Urlaub, E. Käs, A.M. Carothers, L.A. Chasin, Deletion of the diploid dihydrofolate reductase locus from cultured mammalian cells, Cell. 33 (1983) 405–412, https://doi.org/10.1016/0092-8674(83)90422-1.
[67] M. Wigler, A. Pellicer, S. Silverstein, R. Axel, G. Urlaub, L. Chasin, DNA-mediated transfer of the adenine phosphoribosyltransferase locus into mammalian cells, Proc. Natl. Acad. Sci. USA 76 (1979) 1373–1376, https://doi.org/10.1073/pnas.76.3.1373.
[68] E. Macia, M. Ehrlich, R. Massol, E. Boucrot, C. Brunner, T. Kirchhausen, Dynasore, a Cell-Permeable Inhibitor of Dynamin, Dev. Cell. 10 (2006) 839–850, https://doi.org/10.1016/j.devcel.2006.04.002.
[69] D. Vercauteren, R.E. Vandenbroucke, A.T. Jones, J. Rejman, J. Demeester, S.C. De Smedt, N.N. Sanders, K. Braeckmans, The use of inhibitors to study endocytic pathways of gene carriers: Optimization and pitfalls, Mol. Ther. 18 (2010) 561–569, https://doi.org/10.1038/mt.2009.281.
[70] H.-P. Lin, B. Singla, P. Ghoshal, J.L. Faulkner, M. Cherian-Shaw, P.M. O'Connor, J.-X. She, E.J. Belin de Chantemele, G. Csányi, Identification of novel macropinocytosis inhibitors using a rational screen of Food and Drug Administration-approved drugs, Br. J. Pharmacol. 175 (2018) 3640–3655, https://doi.org/10.1111/bph.14429.
[71] C.J. Ciudad, G. Urlaub, L.A. Chasin, Deletion analysis of the Chinese hamster dihydrofolate reductase gene promoter, J. Biol. Chem. 263 (1988) 16274–16282. http://www.jbc.org/content/263/31/16274.short.
[72] X. Villalobos, L. Rodríguez, J. Prévot, C. Oleaga, C.J. Ciudad, V. Noé, Stability and Immunogenicity Properties of the Gene-Silencing Polypurine Reverse Hoogsteen Hairpins, Mol. Pharm. 11 (2014) 254–264, https://doi.org/10.1021/mp400431f.
[73] C. Pichon, L. Billiet, P. Midoux, Chemical vectors for gene delivery: uptake and intracellular trafficking, Curr. Opin. Biotechnol. 21 (2010) 640–645, https://doi.org/10.1016/j.copbio.2010.07.003.
[74] P. Dubruel, B. Christiaens, B. Vanloo, K. Bracke, M. Rosseneu, J. Vandekerckhove, E. Schacht, Physicochemical and biological evaluation of cationic polymethacrylates as vectors for gene delivery, Eur. J. Pharm. Sci. 18 (2003) 211–220, https://doi.org/10.1016/S0928-0987(02)00280-4.
[75] O. Petrichenko, M. Rucins, A. Vezane, I. Timofejeva, A. Sobolev, B. Cekavicus, K. Pajuste, M. Plotniece, M. Gosteva, T. Kozlovska, A. Plotniece, Studies of the physicochemical and structural properties of self-assembling cationic pyridine derivatives as gene delivery agents, Chem. Phys. Lipids. 191 (2015) 25–37, https://doi.org/10.1016/j.chemphyslip.2015.08.005.
[76] K. Pajuste, Z. Hyvönen, O. Petrichenko, D. Kaldre, M. Rucins, B. Cekavicus, V. Ose, B. Skrivele, M. Gosteva, E. Morin-Picardat, M. Plotniece, A. Sobolev, G. Duburs, M. Ruponen, A. Plotniece, Gene delivery agents possessing antiradical activity: Self-assembling cationic amphiphilic 1,4-dihydropyridine derivatives, New J. Chem. 37 (2013) 3062–3075, https://doi.org/10.1039/c3nj00272a.
[77] M. Zhang, J.J. Coen, Y. Suzuki, M.R. Siedow, A. Niemierko, L.Y. Khor, A. Pollack, Y. Zhang, A.L. Zietman, W.U. Shipley, A. Chakravarti, Survivin is a potential mediator of prostate cancer metastasis, Int. J. Radiat. Oncol. Biol. Phys. 78 (2010) 1095–1103, https://doi.org/10.1016/j.ijrobp.2009.09.007.
[78] X. Cai, S. Ma, M. Gu, C. Zu, W. Qu, X. Zheng, Survivin regulates the expression of VEGF-C in lymphatic metastasis of breast cancer, Diagn. Pathol. 7 (2012) 52, https://doi.org/10.1186/1746-1596-7-52.
[79] G.H. Lee, Y.E. Joo, Y.S. Koh, I.J. Chung, Y.K. Park, J.H. Lee, H.S. Kim, S.K. Choi, J. S. Rew, C.S. Park, S.J. Kim, Expression of survivin in gastric cancer and its relationship with tumor angiogenesis, Eur. J. Gastroenterol. Hepatol. 18 (2006) 957–963, https://doi.org/10.1097/01.meg.0000230086.83792.56.
[80] K. Miyachi, K. Sasaki, S. Onodera, T. Taguchi, M. Nagamachi, H. Kaneko, M. Sunagawa, Correlation between survivin mRNA expression and lymph node metastasis in gastric cancer, Gastric Cancer. 6 (2003) 217–224, https://doi.org/10.1007/s10120-003-0255-2.
[81] L. Zhang, Y. Ye, D. Yang, J. Lin, Survivin and vascular endothelial growth factor are associated with spontaneous pulmonary metastasis of osteosarcoma: Development of an orthotopic mouse model, Oncol. Lett. 8 (2014) 2577–2580, https://doi.org/10.3892/ol.2014.2556.
[82] T. Azuhata, D. Scott, S. Takamizawa, J. Wen, A. Davidoff, M. Fukuzawa, A. Sandler, The inhibitor of apoptosis protein survivin is associated with high-risk behavior of neuroblastoma, J. Pediatr. Surg. 36 (2001) 1785–1791, https://doi.org/10.1053/jpsu.2001.28839.
[83] R. Ito, S. Asami, S. Motohashi, S. Ootsuka, Y. Yamaguchi, M. Chin, H. Shichino, Y. Yoshida, N. Nemoto, H. Mugishima, T. Suzuki, Significance of survivin mRNA expression in prognosis of neuroblastoma, Biol. Pharm. Bull. 28 (2005) 565–568, https://doi.org/10.1248/bpb.28.565.
[84] H. Liang, L. Zhang, R. Xu, X.L. Ju, Silencing of survivin using YM155 induces apoptosis and chemosensitization in neuroblastomas cells, Eur. Rev. Med. Pharmacol. Sci. 17 (2013) 2909–2915 (accessed January 5, 2021), https://www.europeanreview.org/article/5826.